

## Photon-echo quantum beats on the $7P_{3/2}$ - $6S_{1/2}$ transition in cesium

Steven Aoki\*

*Ryerson Physical Laboratory, Department of Physics, University of Chicago, Chicago, Illinois 60637*

(Received 27 October 1978)

Photon-echo quantum beats arising from magnetic splitting of the cesium  $7P_{3/2}$ - $6S_{1/2}$  transition were observed in a dilute atomic vapor by means of a novel polarization-rotation technique. The quantum-beat spectrum contains frequencies generated by the hyperfine structure of the  $7P_{3/2}$  level as well as those due to the Zeeman splitting of both ground and excited levels. Experimental data for both  $F = 3$  and  $F = 4$  hyperfine components of the  $6S_{1/2}$  ground state and for several echo delay times were fitted to calculated spectra, including corrections arising from Faraday rotation of the echo pulses.

### I. INTRODUCTION

Photon-echo experiments, which study the time evolution of a coherent superposition of atomic or molecular states, have proved to be a sensitive probe of relaxation process in a number of solid and gaseous media.<sup>1-3</sup> In many cases, the levels which participate in the echo are characterized by small fine-structure, hyperfine, or Zeeman splittings which cause modulations, or quantum beats, in the echo signal.<sup>4,5</sup> For such systems, a detailed analysis of multilevel echo dynamics is necessary in any treatment of relaxation processes; a simple two-level description of the photon echo is inadequate.

This paper reports new experimental data on echo quantum beats generated by hyperfine and magnetic splitting of the  $7P_{3/2}$ - $6S_{1/2}$  transition in cesium. The small magnitude of the  $7P_{3/2}$  hyperfine structure permits observation of echo modulations in both the hyperfine Zeeman and hyperfine Paschen-Back regimes, testing the theoretical description of echoes in multilevel systems. The experimental procedure exploits the photon-echo polarization rotation reported by Baer and Abella,<sup>6</sup> who observed echoes emitted by a cesium sample subjected to an axial magnetic field whose polarization was orthogonal to that of the excitation pulses. Use of this novel technique yields a spectrum of echo intensity which shows strong modulations as a function of applied magnetic field strength, at the same time greatly simplifying laboratory observation of photon echoes. The polarization-rotation effect arises from interference between the magnetic sublevels of the states generating the echo, and is therefore a form of quantum beat.

To illustrate the relationship between echo polarization rotation and quantum beats, we consider the hypothetical energy-level diagram of Fig. 1(a). The states are labeled by quantum numbers  $|J, M\rangle$ . The excited state is assumed to have total angular

momentum  $J = 1$ , and to be split by a weak magnetic field into components corresponding to  $M = \pm 1, 0$ ; the ground state has  $J = 0$ , and hence is nondegenerate. As only  $\Delta M = \pm 1$  transitions are caused by linearly polarized light propagating parallel to the magnetic field, the  $M = 0$  component of the excited state does not interact with the optical radiation, and is therefore omitted from the diagram.

To generate a photon echo, a pair of laser pulses are applied, separated in time by an interval  $\tau$ . The laser linewidth is assumed to be sufficiently broad as to overlap both Zeeman components.

Although in general both magnetic sublevels of the excited state are populated following illumination with linearly polarized light, we concentrate, for purposes of clarity, on the part of the atomic wave function corresponding to the superposition of  $|1, +1\rangle$  and  $|0, 0\rangle$  represented by Fig. 1(b). In the time interval between the two pulses, the electric dipole moment of this superposition state rotates at angular frequency  $\omega_+$ .

Application of the second laser pulse causes transitions to take place between ground and excited levels, remixing the state prepared by the first pulse. If the action of the second pulse leaves the atom in the original sublevels  $|1, +1\rangle$  and  $|0, 0\rangle$ , as shown in Fig. 1(c), the phase evolution between  $t = \tau$  and  $t = 2\tau$  compensates that between  $t = 0$  and  $t = \tau$ , and no modulation or rotation of the echo results.

An alternative channel is available to the system, however. The second pulse can leave the atom in a superposition of  $|1, -1\rangle$  and  $|0, 0\rangle$ , as shown in Fig. 1(d). The relative orientation of the orbital angular momentum and the Larmor precession are now reversed, causing the electric dipole moment of the superposition state to rotate at a lower angular frequency  $\omega_-$  during the second free-precession period. Thus at time  $t = 2\tau$ , when the echo pulse is generated, the dipole moment shows a net rotation with respect to its initial direction, caus-

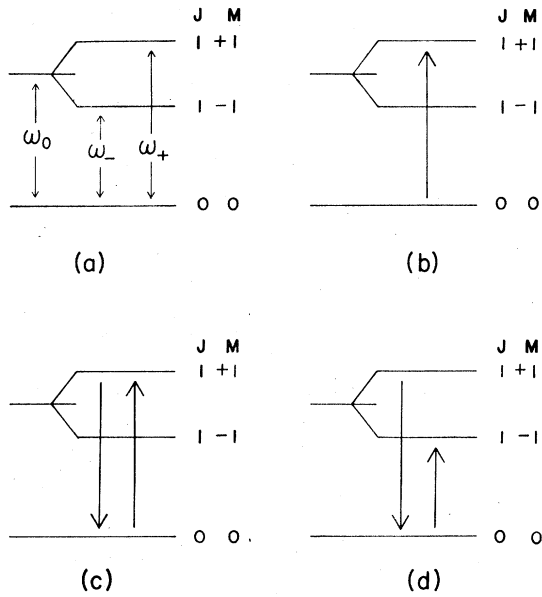


FIG. 1. Hypothetical energy-level diagram. (a) Energy levels for  $J=0$  and  $J=1$  states in weak magnetic field;  $\omega_+$  and  $\omega_-$  denote transition frequencies for right- and left-circularly-polarized light propagating parallel to the magnetic field.

ing a corresponding rotation in the polarization of the emitted light.

Although the above discussion applies to a  $J=0$  to  $J=1$  transition, the argument may be generalized to arbitrary ground- and excited-state angular momenta. The splittings which modulate the echo amplitude can occur in the ground as well as the excited state; in this respect, photon-echo quantum interference phenomena differ from the fluorescence quantum beats observed by Haroche *et al.*<sup>7</sup> As no atom-atom correlations are involved, they differ as well from the collective quantum beats discussed by Chow *et al.* and Herman *et al.*<sup>8</sup> They are closely related, however, to the superfluorescence quantum beats reported by Vreken *et al.*<sup>9</sup>

## II. THEORY

The photon echo is most clearly visualized by treating the atom or molecule under investigation as a two-level system illuminated by a monochromatic laser beam.<sup>10</sup> This approach yields a particularly simple picture of the dynamics of the laser-atom interaction, but is inappropriate for discussion of echo quantum beats and polarization rotation, since it explicitly disregards the level splittings responsible for these quantum interference effects. Lambert *et al.*<sup>11</sup> have derived a suitable formalism for multilevel echo problems, basing their work on the earlier treatment by

Gordon *et al.*<sup>2</sup> of photon echoes generated on highly degenerate molecular transitions. We briefly review this theory as it applies to the present experiment; details of the calculation may be found in Refs. 2 and 11. (Schenzle *et al.*<sup>12</sup> present a different formalism, which is equivalent to that described here for the specific case of on-resonance excitation of a three-level system.)

Consider a pair of ground and excited states  $|\gamma J\rangle$  and  $|\gamma' J'\rangle$  split into sublevels  $|\gamma JM\rangle$  and  $|\gamma' J' M'\rangle$ . In the presence of monochromatic light of frequency  $\omega$  (assumed to be on or near resonance with the transition frequency and linearly polarized along the  $x$  axis), the density matrix  $\sigma$  for such a system obeys the equation of motion

$$i\hbar \frac{d\sigma}{dt} = [\mathcal{H}, \sigma], \quad (1)$$

where

$$\mathcal{H} = \mathcal{H}_0 - 2\vec{p} \cdot \vec{E}(t) \cos \omega t, \quad (2)$$

$\mathcal{H}_0$  is the unperturbed atomic Hamiltonian,  $\vec{p}$  is the electric dipole moment of the atom, and  $\vec{E}(t)$  is the slowly varying envelope of the electric field associated with the applied optical excitation. To remove the rapidly oscillating part of the Hamiltonian, we make the rotating-frame transformation

$$\rho(t) = e^{-iS t} \sigma(t) e^{iS t}, \quad (3)$$

$$i\hbar \frac{d\rho}{dt} = [\hbar\Delta - \vec{p} \cdot \vec{E}, \rho]. \quad (4)$$

$S$  is a diagonal matrix with elements

$$\langle \gamma' M' | S | \gamma' M' \rangle = E_{\gamma'} + \hbar\omega, \quad \langle \gamma M | S | \gamma M \rangle = E_{\gamma} \quad (5)$$

for all  $M$  and  $M'$ , where  $E_{\gamma}$  is the energy of the center of gravity of the ground-state multiplet, and  $\omega = (1/\hbar)(\mathcal{H}_0 - S)$  is the detuning operator.

For a laser pulse initiated at time  $t = t_0$ , Eq. (4) has the solution

$$\rho(t) = U(t - t_0) \rho(t_0) U^{-1}(t - t_0), \quad (6)$$

where the pulse operator  $U(t - t_0)$  is given by

$$U(t - t_0) = \exp[-i\vec{A} \cdot \vec{p}] = \exp\left[-(i/\hbar) \int_{t_0}^t E(t') dt' \cdot \vec{p}\right]. \quad (7)$$

(In the presence of a laser pulse, we neglect  $\hbar\Delta$  in comparison to  $\vec{p} \cdot \vec{E}$ .)

If the optical excitation is turned off at  $t = t_1$ , the subsequent evolution of the density matrix is determined by

$$\rho(t) = e^{-i\Delta(t-t_1)} \rho(t_1) e^{i\Delta(t-t_1)}. \quad (8)$$

The rotating-frame density matrix following a two-pulse echo excitation sequence is therefore found by evaluation of

$$\begin{aligned} \rho(t) = & e^{-i\Delta(t-t_3)}U(t_3-t_2)e^{-i\Delta(t_2-t_1)} \\ & \times U(t_1-t_0)\rho(t_0)U^{-1}(t_1-t_0)e^{i\Delta(t_2-t_1)} \\ & \times U^{-1}(t_3-t_2)e^{i\Delta(t-t_3)}, \end{aligned} \quad (9)$$

where the first pulse is applied between  $t_0$  and  $t_1$  and the second between  $t_2$  and  $t_3$ . The electric dipole moment of the atomic system can then be determined from

$$\langle \vec{p}(t) \rangle = \text{Tr}[\vec{p}\rho(t)] = \text{Tr}[\vec{p}e^{-iSt}\rho(t)e^{iSt}]. \quad (10)$$

The intensity of the echo will be proportional to  $|\langle \vec{p}(t) \rangle|^2$  evaluated at  $t = 2\tau$ , where  $\tau$  is the interval between the two excitation pulses.

Expanding the trace in terms of the energy eigenfunctions  $|\gamma JM\rangle$ , we find

$$\begin{aligned} \langle p(t) \rangle = & \sum_{\substack{JM \\ J'M'}} \langle \gamma JM | p | \gamma' J' M' \rangle \langle \gamma' J' M' | \rho(t) | \gamma JM \rangle \\ & \times e^{-i\omega t} + \text{c.c.} \end{aligned} \quad (11)$$

The density-matrix element

$$\langle \gamma' J' M' | \rho(t) | \gamma JM \rangle$$

is obtained by substitution from Eq. (9); it can be expanded in the same set of eigenfunctions by writing the pulse operators as

$$\vec{U} = (-i\vec{A}\cdot\vec{p}) = \cos(\vec{A}\cdot\vec{p}) - i\sin(\vec{A}\cdot\vec{p}) \quad (12)$$

and noting that

$$\langle \gamma JM | \cos \vec{A}\cdot\vec{p} | \gamma' J' M' \rangle$$

is nonzero only if  $\gamma = \gamma'$ , while

$$\langle \gamma JM | \sin \vec{A}\cdot\vec{p} | \gamma' J' M' \rangle \neq 0$$

requires  $\gamma \neq \gamma'$ .

Retaining only those terms which contribute to the echo, we find

$$\begin{aligned} \langle \vec{p}(t) \rangle = & \frac{e^{-i\omega t}}{2} \sum \exp[\Delta_{J_2M_2, J_1M_1}(t-\tau) - \Delta_{J_4M_4, J_3M_3}\tau] \\ & \times \vec{Q}(J_1M_1; J_2M_2; J_3M_3; J_4M_4) + \text{c.c.}, \end{aligned} \quad (13)$$

$$\vec{Q}(J_2M_2; J_1M_1; J_3M_3; J_4M_4)$$

$$\begin{aligned} = & \langle \gamma J_1M_1 | \vec{p} | \gamma' J_2M_2 \rangle \langle \gamma' J_2M_2 | \sin \vec{A}_1\cdot\vec{p} | \gamma J_3M_3 \rangle \\ & \times \langle \gamma J_3M_3 | \sin 2\vec{A}_2\cdot\vec{p} | \gamma' J_4M_4 \rangle \\ & \times \langle \gamma' J_4M_4 | \sin \vec{A}_1\cdot\vec{p} | \gamma J_1M_1 \rangle. \end{aligned} \quad (14)$$

The summation runs over all values of  $\Delta$ ,  $J$ , and  $M$  for each of the four matrix elements which make up the coefficient  $\vec{Q}$ . The frequencies appearing in the argument of the exponential are defined by

$$\Delta_{JM, J'M'} = (1/\hbar)[E(\gamma JM) - E(\gamma' J' M')],$$

where  $E(\gamma JM)$  is the energy of the sublevel  $|\gamma JM\rangle$ .

$\vec{A}_1$  and  $\vec{A}_2$  are the integrated electric field envelopes of the first and second excitation pulses.

Equation (14) may be greatly simplified if the applied laser pulses are sufficiently weak as to allow the substitution

$$\langle \gamma JM | \sin \vec{A}\cdot\vec{p} | \gamma' J' M' \rangle \approx \vec{A}\cdot\langle \gamma JM | \vec{p} | \gamma' J' M' \rangle. \quad (15)$$

Physically, this weak-field approximation corresponds to neglect of the multiphoton transition processes, represented by the higher-order terms in the power-series expansion of  $\sin \vec{A}\cdot\vec{p}$ , in comparison to the first-order single-photon term. Using approximation (15) and taking the laser polarization to lie along the  $x$  axis, we can write the coefficient  $\vec{Q}$

$$\begin{aligned} \vec{Q}(J_1M_1; J_2M_2; J_3M_3; J_4M_4) \\ = & 2A_x^2 A_2 \langle \gamma J_1M_1 | \vec{p} | \gamma' J_2M_2 \rangle \langle \gamma' J_2M_2 | p_x | \gamma J_3M_3 \rangle \\ & \times \langle \gamma J_3M_3 | p_x | \gamma' J_4M_4 \rangle \langle \gamma' J_4M_4 | p_x | \gamma J_1M_1 \rangle. \end{aligned} \quad (16)$$

With the introduction of spherical components  $p_+ = -\sqrt{\frac{1}{2}}(p_x + ip_y)$  and  $p_- = \sqrt{\frac{1}{2}}(p_x - ip_y)$ ,  $Q_x$  may be seen to be real and  $Q_y$  pure imaginary if the standard phase conventions are assumed whereby the matrix elements of  $p_{\pm}$  are taken to be real. The amplitude of the oscillating electric dipole moment, along the  $x$  and  $y$  axes, corresponding to echo polarization parallel and perpendicular to that of the excitation pulses, will then be

$$\begin{aligned} p_x(t) = & \sum \cos[\Delta_{J_2M_2, J_1M_1}(t-\tau) - \Delta_{J_4M_4, J_3M_3}\tau] \\ & \times Q_x(J_1M_1; J_2M_2; J_3M_3; J_4M_4), \end{aligned} \quad (17)$$

$$\begin{aligned} p_y(t) = & -i \sum \sin[\Delta_{J_2M_2, J_1M_1}(t-\tau) - \Delta_{J_4M_4, J_3M_3}\tau] \\ & \times Q_y(J_1M_1; J_2M_2; J_3M_3; J_4M_4). \end{aligned} \quad (18)$$

As in the simple example discussed above, modulation of the echo amplitude indicated by nonzero arguments of the sine and cosine factors in Eqs. (17) and (18) arises when the first and second excitation pulses connect *different* pairs of sublevels. The  $x$  and  $y$  components of the dipole moment oscillate out of phase corresponding to a rotation of the plane of polarization of the echo. Coefficients  $\vec{Q}$  arising from excitation of the *same* pair of sublevels by the first and second pulses yield zero argument for the trigonometric factors at time  $t = 2\tau$ ;  $p_y$  is then zero, while  $p_x$  assumes a value which is independent of  $\tau$ . The  $x$  component of the echo signal therefore appears as a constant amplitude modulated by quantum interference. This constant background is absent from the  $y$  component.

It must be emphasized that the photon-echo polarization rotation is physically distinct from the Faraday effect. Faraday rotation arises from the

propagation of light through the active medium; the rotation angle is therefore proportional to the optical path length in the sample. The echo polarization rotation is caused by the precession of the atom's dipole moments during the intervals *between* pulses, and is independent of sample path length. Nevertheless, Faraday rotation of both excitation and echo pulses may add an additional small rotation of the echo polarization to that obtained from Eqs. (17) and (18). The intensity of the echo pulse measured by a polarized detector with pass axis along the  $y$  axis will then be

$$I_y \sim |\langle p_y \rangle|^2 \cos^2 \theta_F(H) + |\langle p_x \rangle|^2 \sin^2 \theta_F(H), \quad (19)$$

where  $\theta_F(H)$  is the Faraday rotation angle, and  $\langle p_x \rangle$  and  $\langle p_y \rangle$  are given by Eqs. (17) and (18), corresponding to a mixture of  $x$  and  $y$  components which changes with magnetic field strength.

If the pulse separation  $\tau$  is fixed, but the Zeeman splittings  $\Delta_{J_M, J' M'}$  are varied by sweeping the external magnetic field, the echo quantum beats will be observed as oscillations in the echo intensity as the field is swept. To obtain this spectrum of echo intensity as a function of magnetic field strength requires evaluation of both the coefficients  $\bar{Q}$ , defined by Eq. (14), and the dependence of the frequencies  $\Delta_{J_M, J' M'}$  on the applied field. In the specific instance of the cesium  $7P_{3/2} - 6S_{1/2}$  transition, the hyperfine splittings in the excited state are much smaller than the Doppler width, and hence unresolved. The summations of Eqs. (17) and (18) must therefore be extended over several values of the total angular momentum  $\vec{F} = \vec{I} + \vec{J}$ , introducing modulations at the hyperfine splitting frequencies which persist for zero magnetic field. (The 9.2-GHz ground-state splitting is sufficiently large to allow the  $F = 3$  and  $F = 4$  components to be excited selectively.) The coefficients  $\bar{Q}$  are therefore composed of matrix elements of the form

$$\langle \gamma I J F M_F | p_{\pm} | \gamma' I' J' F' M'_F \rangle,$$

which may be simplified by use of the Wigner-Eckart theorem,<sup>13</sup> and by noting that the dipole moment operator acts only on the electronic part of the state, commuting with the nuclear spin  $\vec{I}$ , we get

$$\begin{aligned} & \langle \gamma I J F M_F | p_{\pm} | \gamma' I' J' F' M'_F \rangle \\ &= (-1)^{F-M_F} \begin{pmatrix} F & 1 & F' \\ -M_F & \pm 1 & M'_F \end{pmatrix} \langle \gamma I J F || p || \gamma' I' J' F' \rangle, \\ & \langle \gamma I J F || p || \gamma' I' J' F' \rangle \\ &= (-1)^{F+I+J'+1} [(2F+1)(2F'+1)]^{1/2} \begin{Bmatrix} I & F' & J' \\ I & J & F \end{Bmatrix} \\ & \times \langle \gamma I J || p || \gamma' I' J' \rangle. \end{aligned} \quad (20)$$

An additional consequence of the small magnitude of the excited-state hyperfine splittings is that a weak magnetic field—5 G or more—suffices to decouple the nuclear spin from the electronic total angular momentum, over the range of magnetic field strengths utilized in this experiment, the frequencies corresponding to a particular coefficient  $\bar{Q}$  ( $J_1 M_1; J_2 M_2; J_3 M_3; J_4 M_4$ ) vary nonlinearly with the magnetic field, and must be obtained by diagonalizing the Hamiltonian:

$$\begin{aligned} \mathcal{H} &= \mathcal{H}_{\text{hyperfine}} + \mathcal{H}_{\text{Zeeman}} \\ &= A \vec{I} \cdot \vec{J} + B \frac{3(\vec{I} \cdot \vec{J})^2 + \frac{3}{2} \vec{I} \cdot \vec{J} - I^2 J^2}{2IJ(2I-1)(2J-1)} - \vec{\mu} \cdot \vec{H}, \end{aligned} \quad (21)$$

where  $A$  and  $B$  are the dipole and quadrupole hyperfine constants. [The frequency difference between the centers of gravity of ground- and excited-state multiplets cancels in each term of Eqs. (17) and (18), and hence may be ignored.] In the  $I J F M_F$  representation the Hamiltonian has matrix elements

$$\langle \gamma I J F M_F | \mathcal{H} | \gamma I J F M_F \rangle = AK + B \frac{3K^2 + \frac{3}{2}K - I(I+1)J(J+1)}{2IJ(2I-1)(2J-1)} - M_F \mu_0 \tilde{H}_z g_J \frac{J(J+1) + F(F+1) - I(I+1)}{2F(F+1)}, \quad (22)$$

$$\begin{aligned} \langle \gamma I J F M_F | \mathcal{H} | \gamma I J F + 1 M_F \rangle &= -\mu_0 \tilde{H}_z g_J [(F + M_F + 1)(F - M_F + 1)]^{1/2} \\ & \times \left( \frac{(I + J + F + 2)(J - 1 + F + 1)(I + J + F + 1)(I + J - F)}{4(2F + 3)(F + 1)^2(2F + 1)} \right)^{1/2} \end{aligned} \quad (23)$$

where

$$K = \frac{1}{2} [F(F+1) - I(I+1) - J(J+1)].$$

(<sup>133</sup>Cs has nuclear spin  $I = \frac{7}{2}$ .) For the  $7P_{3/2}$  ex-

cited state, the matrix elements of Eq. (22) were evaluated using the following experimental values<sup>14</sup> for the hyperfine constants and  $g$  factor:  $A = 16.605$  MHz,  $B = -0.15$  MHz, and  $g_J = 1.3349$ .

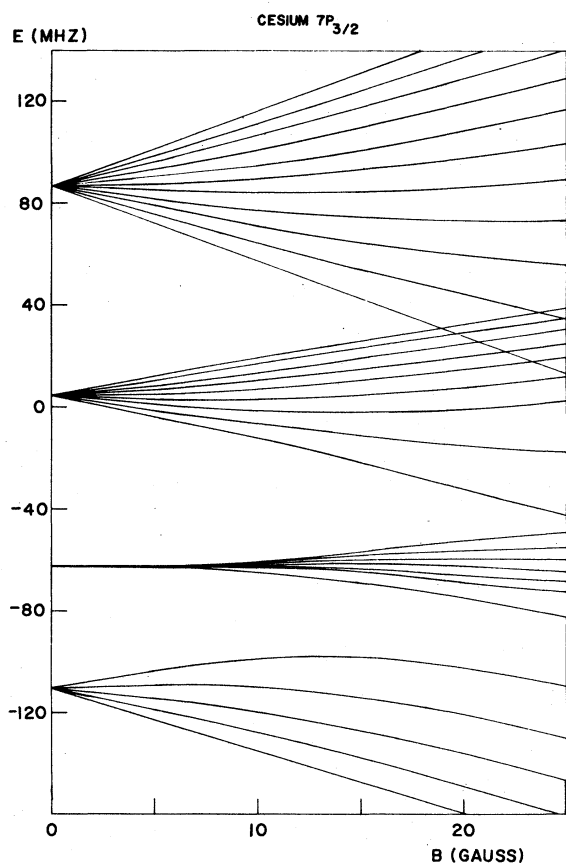


FIG. 2. Level diagram of the cesium  $7P_{3/2}$  state in magnetic field of 0–25 G. The nuclear spin  $I = \frac{7}{2}$ ; hyperfine constants  $A = 16.605$  MHz,  $B = -0.15$  MHz, and  $g$  factor  $g_J = 1.3349$  were obtained from Ref. 14.

Numerical diagonalization of the resulting Hamiltonian yielded the energy levels shown in Fig. 2. As a check of the accuracy of the numerical calculation, the positions of several level crossings were computed, and were found to reproduce correctly the original measurements of Svanberg and Rydberg.<sup>15</sup>

For the  $6S_{1/2}$  ground state, the magnetic splittings are small compared to the zero-field hyperfine structure, and the off-diagonal elements of the Hamiltonian may be neglected. The hyperfine Zeeman energy levels are then obtained directly from Eq. (22), with  $A = 9.1926$  GHz,  $B = 0$ , and  $g_J = 2.003$ . (Values for these constants also taken from Ref. 14.) The frequency differences obtained from the numerical calculation and from Eq. (22) may then be combined with the coefficients  $\bar{Q}$  calculated by means of Eqs. (16) and (20) to evaluate the  $x$  and  $y$  components of the electric dipole moment as a function of applied magnetic field, by means of Eqs. (17) and (18). The spectrum of echo intensity versus magnetic field may then be

obtained from Eq. (19), once the magnitude of the Faraday rotation is determined. In the limit of low sample number density, the Faraday rotation is small, and the echo-intensity spectrum may be found directly by squaring the  $y$  component of the dipole moment.

### III. EXPERIMENTAL PROCEDURE

The apparatus employed is shown schematically in Fig. 3. A Hänsch-design dye laser,<sup>16</sup> pumped by an N.R.G. Inc. nitrogen laser, produced pulses of 5-nsec duration with a peak power of 3 kW at 4555 Å, and a repetition rate of 60 Hz. The linewidth was estimated to be about 3 GHz, readily resolving the 9.2-GHz ground-state hyperfine splitting in cesium. The dye, a  $10^{-3}M$  solution of 7-diethylamino-4-methylcoumarin in ethanol, circulated through a stainless-steel cell with cemented windows. A beam splitter divided the laser output, sending approximately 70% of the intensity to a White-cell optical delay line. A second beam splitter recombined the delayed and undelayed pulses to form a pulse train, collinear to within 1 mrad.

Collinear excitation was chosen to eliminate Doppler dephasing of the echo signal due to non-parallel propagation of the excitation pulses through the gas sample. We show in the Appendix that, if the propagation vectors of the two pulses intersect at an angle  $\alpha$ , the echo signal will be reduced by a factor given by Eq. (A3):

$$\gamma = \exp[-(8\pi^2/\ln 2)(\tau\alpha\Delta_D)^2],$$

where  $\tau$  is the time interval between the pulses and  $\Delta_D$  is the Doppler half-width of the resonant transition.

The pulse train was linearly polarized by a Glan-Thompson prism and passed through the sample

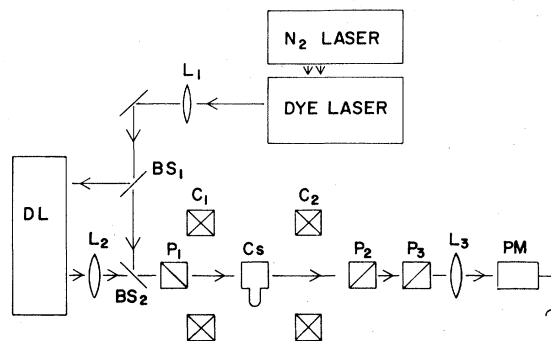


FIG. 3. Experimental schematic. DL is a White-cell delay line; BS<sub>1</sub> and BS<sub>2</sub> beam splitters; C<sub>1</sub> and C<sub>2</sub> Helmholtz coils; P<sub>1</sub>, P<sub>2</sub>, and P<sub>3</sub> Glan-Thompson polarizers; L<sub>1</sub>, L<sub>2</sub>, and L<sub>3</sub> lenses; and PM an RCA 7265 photomultiplier.

cell. The time interval between pulses was varied between 44 and 124 nsec in steps of 20 nsec by adjusting the number of reflections in the delay line. Losses in the beam-handling optics reduced the excitation intensity in each pulse to 10% of the entire dye-laser output. A second Glan-Thompson prism, placed between the sample and the photomultiplier detector with its pass axis orthogonal to the first polarizer, transmitted the rotated echo component, while substantially attenuating the excitation pulses. No electro-optical switching is required. In practice, use of three analyzer prisms yielded the best discrimination between echo and laser pulses. It was also necessary to aperture the detector carefully to minimize pickup of fluorescence and scattered light.

A linear gate sampled the output from the RCA 7265 photomultiplier, accepting only the echo signal. Noise and dark current were rejected by a lower-level discriminator. A fast analog-to-digital converter then determined the echo amplitude. As the dye laser exhibited substantial intensity fluctuations, some 500 to 1000 echo pulses were measured and averaged for each value of magnetic field. In addition to the random shot-to-shot variations, the dye-laser output and frequency tuning often exhibited a slow systematic drift during the 1 to 2 h experimental run. Even though all laser-cavity components and beam-handling optics were securely anchored to a rigid optical table, and a large volume of dye circulated through the laser system, the echo amplitude at fixed magnetic field was observed to fall off by as much as 50% over a period of 2 h. To minimize the effect of this systematic drift on the echo spectrum, the magnet current was repeatedly reset to a standard value, and the corresponding echo amplitude monitored during the course of each experimental run. If the echo signal at the calibration point dropped by more than 20%, data taking was suspended and the laser retuned.

The cesium sample was double-distilled into the sidearm of a 2-cm path-length glass cell, sealed at a background pressure of less than  $10^{-6}$  Torr. A temperature-regulated oven heated the sidearm to  $75 \pm 2^\circ\text{C}$ , corresponding to a number density of about  $10^{12}$   $\text{cm}^{-3}$ . At this density, interatomic collisions have an entirely negligible effect on the photon echo. A separate heater maintained the cell body at approximately  $100^\circ\text{C}$ , preventing cesium condensation on the optical windows. For the  $7P_{3/2} - 6S_{1/2}$  transition at  $4555 \text{ \AA}$ , the absorption length was estimated to be 2 cm.

A pair of Helmholtz coils generated the magnetic field which rotated the echo polarization. Field strengths up to 60 G could be obtained. A  $0.1-\Omega$  precision resistor and digital voltmeter monitored

the current in the coils; regulation of the magnet power supply and water cooling of the coils limited current fluctuations to less than 0.1%. The magnetic field was calibrated as a function of coil current with a Hall-effect gaussmeter and a set of standard magnets.

#### IV. DATA AND DISCUSSION

Figures 4–8 show the measured photon-echo intensity as a function of applied magnetic field strength for both  $F = 3$  and  $F = 4$  ground-state hyperfine components at excitation pulse separations of 43.9, 63.9, and 83.9 nsec. Each datum point represents an average of 500 to 1000 echo pulses; the averaging procedure reduced statistical fluctuations to (10–20)% of the measured amplitude.

The solid lines in Figs. 4–8 represent theoretical spectra calculated by means of the theory presented in Sec. II. As was discussed there, the Faraday effect causes a rotation of the polarization of pulses propagating through the active medium which must be added to the echo polarization rotation, as in Eq. (19). Faraday rotation angles of several degrees were observed for single laser pulses traveling through the cesium sample, even at low values of applied magnetic field. Theoretical determination of the Faraday rotation of intense pulses nearly resonant with a transition between states of high angular momenta entails complicated calculations<sup>17</sup> and requires knowledge of the sample number density, a quantity which is both difficult to measure and unlikely to be uniform along the optical path. Dependence of the Faraday angle on magnetic field strength of the form  $\theta_F(H) = VH$ , where  $V$  is a Verdet constant, was therefore assumed; the best fit to the exper-

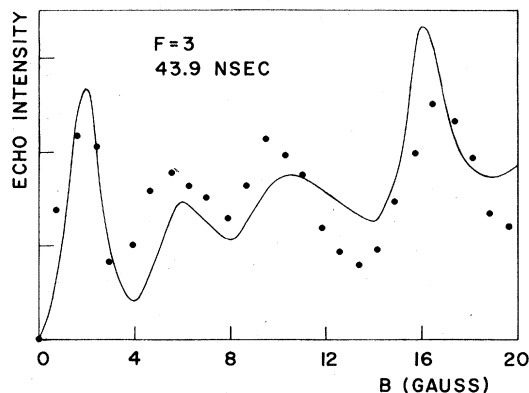


FIG. 4. Echo intensity in arbitrary units vs magnetic field in gauss for  $6S_{1/2}$   $F=3$  ground state, 43.9 nsec pulse separation interval. Experimental data are denoted by solid circles; calculated spectrum by solid line.

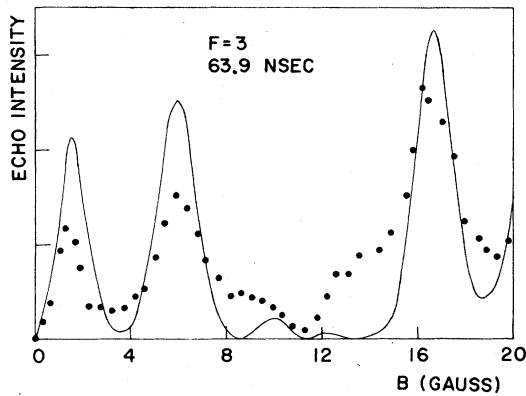


FIG. 5. Echo intensity vs magnetic field for  $F=3$  ground state, 63.9 nsec pulse separation interval.

imental data was obtained for the value  $V = 1.3^\circ/\text{G}$ . Comparable effects arising from Faraday rotation were not observed in a previous photon-echo polarization-rotation experiment on the cesium  $7P_{1/2} - 6S_{1/2}$  transition,<sup>6</sup> as the oscillator strength of this line is smaller by a factor of 4.3 than that of the  $7P_{3/2} - 6S_{1/2}$  line.

Upon taking the Faraday effect into account, we find that the calculated spectra of echo intensity versus magnetic field fit the experimental data well, reproducing the major spectral features for all delay times investigated. As can be seen from Figs. 4–8, the echo spectrum does not scale with the product  $B\tau$ , as was observed for the  $6S_{1/2} - 7P_{1/2}$  transition. The breakdown of this scaling behavior is a consequence of the nonlinear dependence of the energy of the magnetic sublevels on field strength as the atom passes from the hyperfine Zeeman to the hyperfine Paschen-Back regimes.

Several small peaks in the experimental spectra do not appear in the theoretical curves. A possible

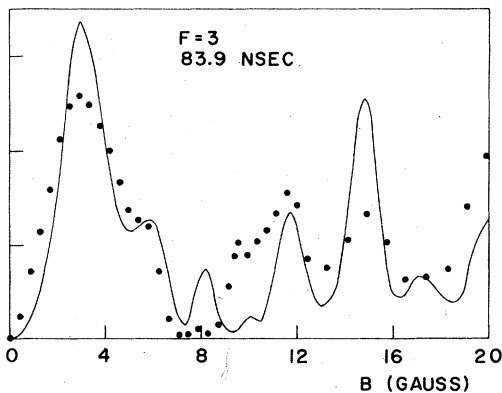


FIG. 6. Echo intensity vs magnetic field for  $F=3$ , 83.9-nsec pulse separation interval.

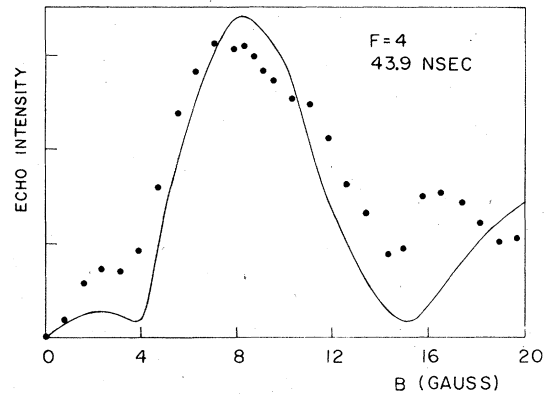


FIG. 7. Echo intensity vs magnetic field for  $F=4$ , 43.9-nsec pulse separation interval.

explanation is that the excitation pulses are sufficiently intense that Eq. (15) is no longer correct. When the attenuation of the laser pulses by the delay line and beam-handling optics is accounted for, an estimate of the pulse area  $\theta = \vec{A} \cdot \langle \vec{p} \rangle$  yields  $\theta \approx 20^\circ$  for a laser peak power of 2 kW, suggesting that the validity of this linear approximation may be somewhat marginal ( $\langle \vec{p} \rangle$  is the reduced dipole matrix element for the  $6S_{1/2} - 7P_{3/2}$  transition). An experimental comparison of the echo spectrum for full laser intensity with that obtained with both laser pulses attenuated by 40% tends, however, to support the use of this approximation, as the sole effect of reducing laser power appears to be a proportionate reduction in echo intensity.

A second possible explanation of the additional peaks in the experimental data is incomplete resolution by the dye laser of the 9-GHz ground-state hyperfine splitting. Overlap of the wings of the laser line with the nonresonant ground-state component could mix additional frequencies into the sum of Eq. (17), since the dipole moment operator

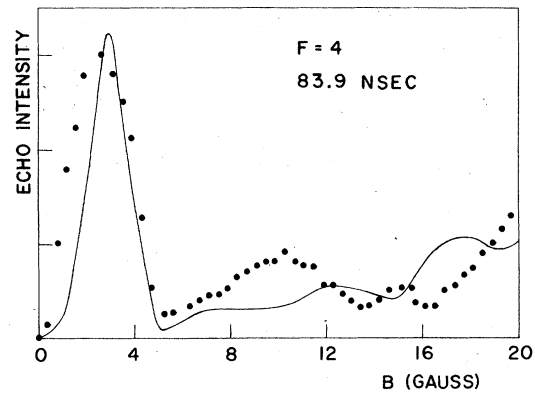


FIG. 8. Echo intensity vs magnetic field for  $F=4$ , 83.9-nsec pulse separation interval.

connects the  $F = 3$  and  $F = 4$  ground states to different sets of excited-state hyperfine sublevels. In point of fact, the theoretical treatment employed neglects both the finite width of the laser line and the degeneracy of ground and excited states during the application of the laser pulses. Linewidth and off-resonance driving effects may, in fact, significantly influence the behavior of the photon echo.

### V. CONCLUSION

A new photon-echo polarization-rotation procedure makes possible observation of photon-echo quantum beats in the form of highly detailed spectra of echo intensity as a function of applied axial magnetic field strength. Such experimental spectra, obtained on the cesium  $7P_{3/2} - 6S_{1/2}$  transition, are correctly predicted by a calculation based on the theoretical work of Lambert *et al.*<sup>11</sup> over a range of magnetic field values characterized by a highly nonlinear dependence of the excited-state magnetic splittings on field strength. The  $F = 3$  and  $F = 4$  ground-state hyperfine components were selectively excited, and a number of different excitation pulse intervals investigated. The agreement obtained between experiment and theory in a system possessing a complex and finely spaced level structure confirms the interpretation of the echo polarization-rotation effect as a quantum interference phenomenon.

Although the present experiment did not encompass high-precision measurements, the dependence of the echo quantum-beat spectrum on both ground- and excited-state  $g$  factors and hyperfine constants suggests that this technique may be useful in the future determination of these quantities, particularly in short-lived excited states. Polarization-rotation studies of echo quantum beats may also find application to the investigation of collisional relaxation processes in gases, as spin-dependent interactions may produce observable changes in the echo quantum-beat structure. Photo-echo relaxation work may also profit from the great simplification of the laboratory setup introduced by the echo polarization-rotation method.

### APPENDIX: DOPPLER DAMPING OF PHOTON ECHOES FOR NONCOLLINEAR EXCITATION

In a gaseous sample, the thermal motion of the excited atoms damps the photon-echo intensity unless the excitation pulses propagate collinearly. Let  $\vec{e}_1$ ,  $\vec{e}_2$ , and  $\vec{e}$  be unit vectors along the directions of propagation of the first, second, and echo pulses. If  $\alpha$  denotes the angle between  $\vec{e}_1$  and  $\vec{e}_2$ , the phase-matching condition  $\vec{e} = \vec{e}_1 - 2\vec{e}_2$  causes the echo to be emitted<sup>1</sup> at an angle  $2\alpha$  with respect

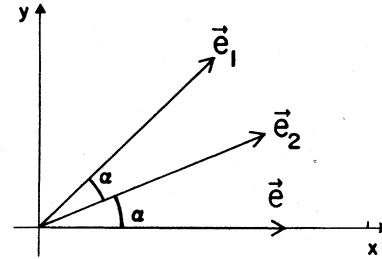


FIG. 9. Echo generation for noncollinear excitation. The first excitation pulse propagates parallel to unit vector  $\vec{e}_1$  and the second along  $\vec{e}_2$ , while the echo is emitted along  $\vec{e}$ .

to  $\vec{e}_1$ , as shown in Fig. 9. An atom moving perpendicularly to  $\vec{e}$  with velocity  $v$  at the time of arrival of the first pulse will then have a velocity component  $v \cdot \sin\alpha$  along  $\vec{e}_2$ , advancing or delaying the arrival time of the second pulse by  $(v/c)\tau \sin\alpha$ , where  $\tau$  is the pulse separation interval seen by a stationary atom. The moving and stationary atoms therefore rephase at slightly different times, and their radiation along  $\vec{e}$  will interfere destructively, reducing the echo signal.

An estimate of the severity of this effect may readily be obtained from a calculation of Scully *et al.*<sup>18</sup> For a small sample, confined to a volume  $V$  near the origin, the expression derived by these authors for the macroscopic dipole moment of a Doppler-broadened system, subsequent to a two-pulse echo-excitation sequence, can be reduced to

$$P(t) = \langle p \rangle \sum_j^n \cos \left[ \omega \left( 1 + \frac{\vec{v}_j \cdot \vec{e}}{c} \right) \left( t - 2\tau - \frac{R}{c} \right) + 2\omega\tau \frac{\vec{v}_j \cdot (\vec{e} - \vec{e}_1)}{c} \right], \quad (\text{A1})$$

where  $\langle p \rangle$  is the expectation value of the electric dipole moment created by the two laser pulses,  $\vec{v}_j$  the velocity of the  $j$ th atom,  $\omega$  the resonance frequency of a stationary atom, and  $R$  the distance to the observation point. Terms of order  $v_j^2/c^2$  have been neglected.

The assumption of a small sample volume is made in order to isolate the Doppler damping mechanism, which is specific to echoes generated in gases. Consideration of extended samples introduces additional interference effects, previously described by Abella *et al.*<sup>1</sup> and by Allen and Eberly,<sup>10</sup> which tend to reduce the echo intensity for large angular separation of the excitation pulses. Such an intensity reduction, whose magnitude is determined by the geometry of the excitation region, acts independently of the Doppler damping discussed here, and is equally present in solid and gaseous samples of equivalent dimensions.

Replacing the sum over  $n$  atoms with an integra-

tion over the Maxwell-Boltzman distribution, and making the assumption that the angle  $\alpha$  is sufficiently small that  $\sin\alpha \approx \alpha$ , we evaluate Eq. (A1) as

$$P = n\langle p \rangle \left( \frac{m}{2\pi kT} \right)^{3/2} \times \int e^{-mv^2/2kT} \cos \left[ S\omega \left( 1 + \frac{v_x}{c} - \frac{4\tau}{cS} \alpha v_y \right) \right] d^3v d^3r \\ = N\langle p \rangle \exp \left( -\frac{\pi^2}{4 \ln 2} S^2 \Delta_D^2 \right) (\cos \omega S) \\ \times \exp \left( -\frac{4\pi^2}{\ln 2} (\tau \alpha \Delta_D)^2 \right), \quad (\text{A2})$$

where  $S = t - 2 - R/c$ , and where the Doppler width

$$\Delta_D = \frac{(2 \ln 2)^{1/2} \omega}{\pi} \left( \frac{kT}{m} \right)^{1/2}$$

and the number density  $N = n/V$  have been introduced. The unit vectors  $\vec{e}$ ,  $\vec{e}_1$ , and  $\vec{e}_2$  have been taken to lie in the  $x$ - $y$  plane, with  $\vec{e}$  aligned along the  $x$  axis.

From the first exponential factor and the cosine term, it may be seen that the macroscopic polarization, which oscillates at frequency  $\omega$ , reaches a maximum amplitude for  $S = 0$ , corresponding to the emission of an echo pulse at time  $t = 2\tau$ . The sec-

ond exponential term causes the echo to damp sharply as the angle between the two excitation pulses is increased. Since the echo intensity is proportional to the square of the macroscopic dipole moment, the signal damping factor  $\gamma$  will be

$$\gamma = \exp[-(8\pi^2/\ln 2)(\tau \alpha \Delta_D)^2]. \quad (\text{A3})$$

For the cesium  $7P_{3/2} - 6S_{1/2}$  transition with a sample temperature of  $100^\circ\text{C}$ , the Doppler width is 0.79 GHz. Taking  $\tau = 44$  nsec (the shortest delay time available experimentally), we get  $\gamma = 0.88$  for  $\alpha = 1$  mrad. and  $\gamma = 0.033$  for  $\alpha = 5$  mrad. The Doppler dephasing of the echo intensity is thus quite severe, even for very small angles. This result suggests that use of collinear excitation may be quite advantageous for photon-echo experiments in atomic vapors.

#### ACKNOWLEDGMENTS

The author wishes to express his gratitude to Professor I. D. Abella for the continual support and encouragement of this research, and to thank Tom Baer for many interesting and useful discussions. This work was supported by the National Science Foundation under Grant No. DMR 77-17546. This paper has been submitted to the Department of Physics, University of Chicago, in partial fulfillment of the requirements for the Ph.D. degree.

\*Present address: University of California, Lawrence Livermore Laboratory, P. O. Box 808, Livermore, Calif. 94550.

<sup>1</sup>I. D. Abella, N. A. Kurnit, and S. R. Hartmann, *Phys. Rev.* **141**, 391 (1966).

<sup>2</sup>J. P. Gordon, C. H. Wang, C. K. N. Patel, R. E. Slusher, and W. J. Tomlinson, *Phys. Rev.* **179**, 294 (1969).

<sup>3</sup>P. R. Berman, J. M. Levy, and R. G. Brewer, *Phys. Rev. A* **11**, 1668 (1975); T. J. Aartsma and D. A. Wiersma, *Phys. Rev. Lett.* **36**, 1360 (1976); T. Baer and I. D. Abella, *Phys. Lett. A* **59**, 371 (1976); B. Bölinger, L. Baede, and H. M. Gibbs, *Opt. Commun.* **18**, 67 (1976).

<sup>4</sup>I. D. Abella, A. Compaan, and L. Q. Lambert, in *Laser Spectroscopy*, edited by R. G. Brewer (Plenum, New York, 1974).

<sup>5</sup>R. L. Shoemaker and F. A. Hopf, *Phys. Rev. Lett.* **33**, 1527 (1974); P. F. Liao, P. Hu, R. Leigh, and S. R. Hartmann, *Phys. Rev. A* **9**, 332 (1974).

<sup>6</sup>T. Baer and I. D. Abella, *Phys. Rev. A* **16**, 2093 (1977).

<sup>7</sup>S. Haroche, J. A. Paisner, and A. L. Schawlow, *Phys. Rev. Lett.* **30**, 948 (1973); S. Haroche, in *High-Resolution Laser Spectroscopy*, edited by K. Shimoda (Spring-

er, Berlin, 1976).

<sup>8</sup>W. W. Chow, M. O. Scully, and J. O. Stoner, *Phys. Rev. A* **11**, 1380 (1975); R. M. Herman, H. Grotch, R. Kornblith, and J. H. Eberly, *ibid.* **11**, 1389 (1975).

<sup>9</sup>Q. H. Vrethen, H. M. J. Hiksloops, and H. M. Gibbs, *Phys. Rev. Lett.* **38**, 764 (1977).

<sup>10</sup>L. Allen and J. H. Eberly, *Optical Resonance and Two-Level Atoms* (Wiley, New York, 1975).

<sup>11</sup>L. Q. Lambert, A. Compaan, and I. D. Abella, *Phys. Rev. A* **4**, 2022 (1971).

<sup>12</sup>A. Schenzle, A. Grossman, and R. G. Brewer, *Phys. Rev. A* **13**, 1891 (1976).

<sup>13</sup>A. Messiah, *Quantum Mechanics* (North-Holland, Amsterdam, 1966), Vol. 2, Appendix C.

<sup>14</sup>E. Arimondo, M. Inguscio, and P. Violino, *Rev. Mod. Phys.* **49**, 31 (1977).

<sup>15</sup>S. Svanberg and S. Rydberg, *Z. Phys.* **227**, 216 (1969).

<sup>16</sup>T. W. Hänsch, *Appl. Opt.* **11**, 895 (1972).

<sup>17</sup>Y. J. Yu and R. K. Osborn, *Phys. Rev. A* **15**, 2404 (1977); N. L. Manakov and V. D. Ovsyannikov, *Sov. J. Quantum Electron.* **5**, 1055 (1975).

<sup>18</sup>M. Scully, M. J. Stephen, and D. C. Burnham, *Phys. Rev.* **171**, 213 (1968).